異常地殻変動検出手法の開発

AUTHOR(S):

佐藤, 一敏; 橋本, 学; 細, 善信

CITATION:

佐藤, 一敏 ...[et al]. 異常地殻変動検出手法の開発. 京都大学防災研究所年報. C 2006, 49(C): 197-209

ISSUE DATE:

2006-04-01

URL:

http://hdl.handle.net/2433/26688

京都大学防災研究所年報 第 49 号 C 平成 18 年 4 月
Annuals of Disas. Prev. Res. Inst., Kyoto Univ., No. 49 C, 2006

Development of a Monitoring Technique of Anomalous Crustal Deformations

Kazutoshi SATO, Manabu HASHIMOTO, and Yoshinobu HOSO

Synopsis

We are taking with the development of the technique which detects the anomalous crustal deformation by using GPS now. The static positioning method which used a daily solution was the main stream with the positioning which used GPS till now. However, the short-term change can't be caught in this method. So, we think that the kinematic GPS positioning method being used for the moving object was applied. But, we must remove various error factors which exist in this technique. As for the short baseline which went until last year, we could remove the influences of the ionospheric and tropospheric delay, and the positioning accuracy is +/- 1 cm. We extend a baseline more this year. We succeed in removing the error factors from the sky by using a spatial filter, and we can get the same result as the short baseline. And we must remove the error to result from the satellite orbit to monitor it in real time. As that result, a large difference wasn't seen in the positioning accuracy which satellite orbit announced from IGS was used.

Keywords: ionospheric and tropospheric delay, moving average, spatial filter, satellite orbit

1. Introduction

The anomalous vertical deformation preceding the 1944 Tonankai Earthquake was detected by leveling survey performed near Kakegawa, Japan, about 300 km away from its epicenter (Mogi, 1982, 1985). He analyzed the leveling data and concluded that there was a more than 10 micro-rad anomalous accelerating tilt change within 1 day before the earthquake. On the other hand, we cannot identify displacements from subsequent earthquakes which occurred within 1 day. Earthquake swarms (e.g., the 1993 Izu swarms, the 1994 Inagawa swarms), aftershock activities (e.g., the 2003 Tokachi-oki earthquake, the 2004 Niigata Chuetsu earthquake), and so on. However, it is hard to detect such a deformation with conventional surveys, because they cover a small area and cannot be frequently made.

We think that an anomalous crustal deformation can be caught by using continuous GPS observation. At present, GSI adopt static GPS for the calculation of daily coordinates of stations. In static GPS, an average coordinate during a certain period is calculated. Its accuracy is now few mm for horizontal and 10-20 mm for vertical components, respectively. GSI is providing daily static solutions of all the stations by analyzing 24 hours data. However the above anomalous deformation completed within 1 day. Static GPS presently adopted can give us only one data per day. Therefore it is important to develop a method to detect such a deformation with GPS. We must adopt a kinematic GPS positioning.

A difference in the static positioning and the kinematic positioning is mentioned briefly here (Table 1). There is a large difference between these two methods in the way that a position is determined, though both positioning are relative positioning. In relative positioning, we take a difference of carrier phases received at two points, uncertainties of wavelength multiplied by arbitrary integer arise in estimate of solution. This uncertainty is called integer ambiguity, or

Table 1 The difference between static GPS positioning and kinematic GPS positioning

	Static Analysis	Kinematic Analysis
Observation Method	All points simultaneously	One by one
Observation Time	0.5 – several hours	Less than several seconds per point
Measurement Baseline	One or more	Only one (reference to rover)
Positioning Determination Method	Movement of satellites	Initialize setting

integer bias. There are many possible solutions which consist of lattice points that are apart from each other with a wavelength of carrier phase. These points change their position according to a satellite's motion gradually. But, there must be a point that does not move. This is the true solution we seek. On the other hand, after initial position is calculated in the similar way to static positioning, a position relative to the reference point is determined by counting the wave numbers in kinematic positioning. There is a restriction to determine initial value again when a cycle slip occurs and the number of waves cannot be counted precisely.

The main purpose of kinematic GPS is positioning of moving objects. For example, it is adopted as a mean of positioning of the ship in the ocean bottom crustal movement observation at present. Error factors must be clarified in advance to measure a position with the accuracy of cm on the ocean. Comparison with the true position of the short baseline (baseline length 43 km), and the long baseline (165 km) was done by fixing the rover (Obana et al., 1999). As a result, they confirmed that an error from the true position is found to be of the order of cm even in case of a long baseline if the condition of the satellite alignment is good. A search for error factors which depends on the baseline length and the estimate of the error were done to solve this (Sato, 2002). In this experiment, many baselines with different length were prepared, and the movement of the moving antenna relative to each reference point was caught, and its deviation from the "true" position that was measured for the zero baselines was evaluated. As a result, a systematic error grows large in proportional to the square of baseline length. Especially when baseline length exceeds 50 km, a systematic error in kinematic analysis grows significantly larger than that in static analysis.

The main error factors are the ionospheric and tropospheric delays. Radio waves surely pass through the ionosphere and the troposphere while they travel from the satellite to the observation points on the ground. The ionosphere has the inhomogeneity of the density, and each size is estimated to be about 10 km (Tsuchiya and Tsuji, 1995). The carrier phase which passed through the ionosphere of the same density reaches almost at the same time. But, a difference arises in arrival time while the carrier phase which passed the ionosphere of the different density. When a baseline length exceeds 10 km, the kinematic GPS is not considered to be applicable since it is impossible to determine bias rapidly (Lachapelle et al., 1992).

Also, there are studies that used kinematic analysis for the monitoring of the volcanic eruption recently (Larson et al., 2001; Irwan et al., 2003). However, the amount of precursory movements is much smaller than that of displacement associated with volcanic eruptions.

There is an example that seismic wave from the 1999 Hector Mine earthquake in Southern California was caught by the SCIGN net (Nikolaidis et al., 2001) and the seismic wave from the 2002 Denali earthquake in Alaska was also caught by the TriNet in Los Angeles Basin (Larson et al., 2003; Bock et al., 2004). Shifts are seen between the displacement detected by 1-Hz GPS and the displacement integrated from the wave from data of the seismometer (Larson et al., 2003).

Therefore, we examine several error factors in the kinematic GPS positioning of the fixed point on land and pursue a method to reduce them in order to achieve the same accuracy as that for the static GPS positioning.

2. The experiment of the detection of virtual slow events with short baseline lengths

2.1 Outline of experiment and data analysis

We developed a sliding table which simulates slow events (Fig. 1). We adopted the mechanism of the drum-type recorder and improved a gear ratio and so on. A GPS antenna can be held on the screw that moves at three constant speeds, such as 0.4, 0.2, and 0.1 mm/min. We also installed a voltage-type displacement gauge parallel to this screw to measure the position of the GPS

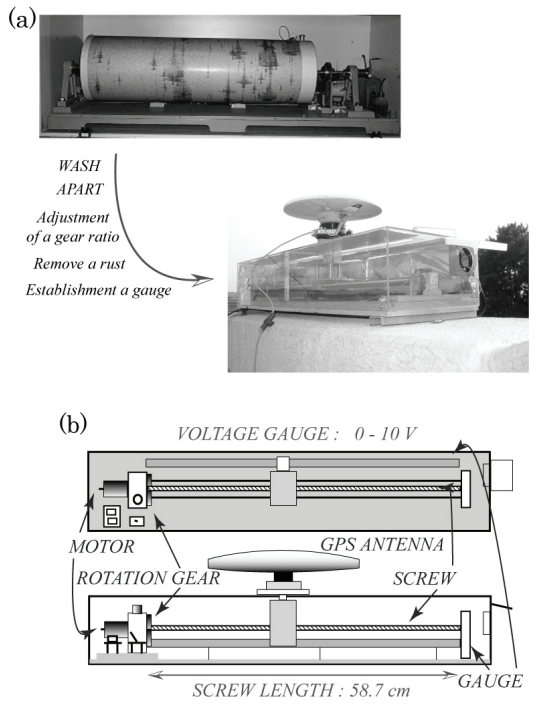

Fig. 1 The development process and the mechanism of a sliding table which simulates slow events.

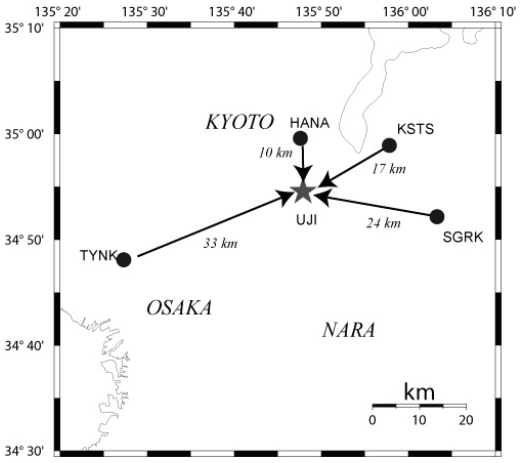

Fig. 2 Baseline map of this experiment. Solid circles are reference points (HANA, KSTS, SGRK, and TYNK), and the solid star is a sliding table (UJIM) and zero baseline reference point (UJIC).

Table 2 Baseline vectors from sliding table (UJIM)

Baseline	North (m)	East (m)	Horizontal (m)
UJIM to UJIC	-5.667	0.511	5.690
UJIM to HANA	9307.863	-469.043	9319.673
UJIM to KSTS	8066.234	15108.577	17126.974
UJIM to SGRK	-6067.999	28006.709	28656.524
UJIM to TYNK	-11897.583	-31405.487	33583.584

antenna. Then, we compared both positions of the GPS antenna determined by the kinematic GPS analysis and by the gauge. We determined the position of antenna from several reference sites located within the range of 0-40 km in different directions in order to see the dependence on direction and distance (Fig. 2 and Table 2).

We verified the effect of the stabilization of the receiver clock by the external frequency standard, NEC Rb-5000A and Rb-3100A at the reference points. The GPS receivers and antennas which used in all reference points are the same, Ashtech Choke-ring antenna with SCIGN radome.

Observed data were analyzed with static analysis to obtain an apriori value of each observation point using the GIPSY/OASIS-II software version 2.6 (Lichten et al., 1987; Zumberge et al., 1997) with precise ephemerides and Earth rotation parameters provided by the Jet Propulsion Laboratory (JPL). As for the kinematic analysis, TRACK which is the kinematic analysis mode of GAMIT software ver.10.07. was used (King et al., 2002). Kalman filter is adopted as the basis of the analysis algorithm both softwares. In the GIPSY software, it is dealing with a carrier phase directly, and

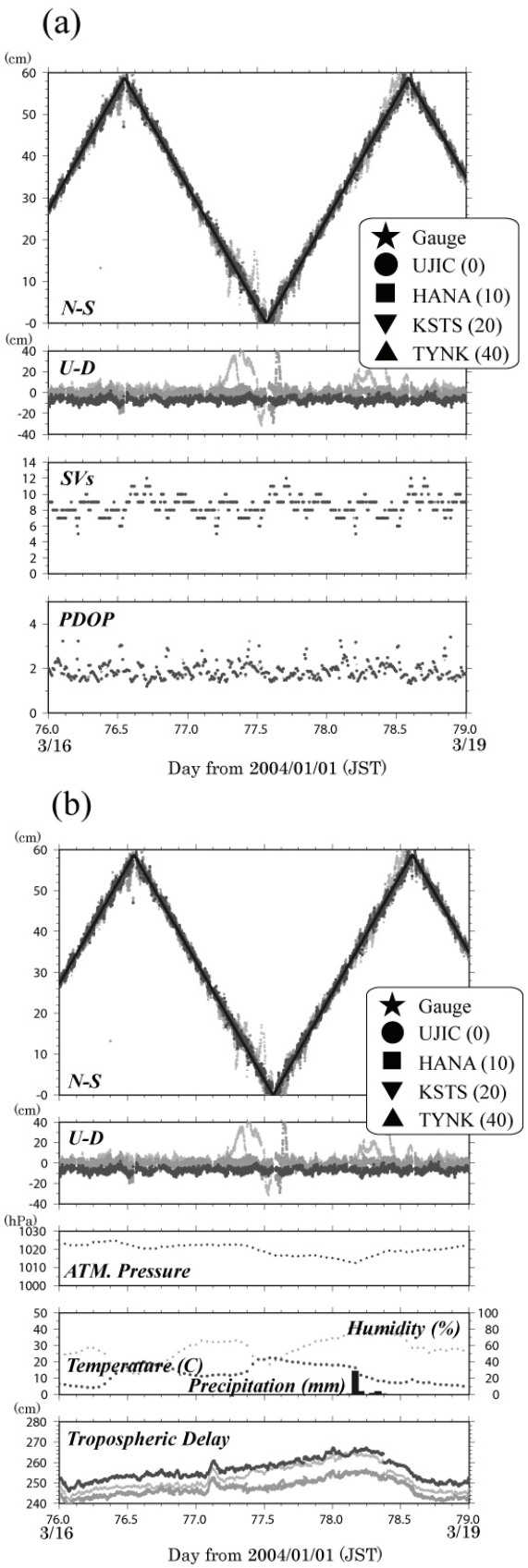

Fig 3. Correlation between kinematic GPS solutions and (a) satellite information, the number of tracked satellites and alignment, (b) the ground weather components.

the amount of the tropospheric delay, a clock error, and so on are estimated at the same time. In TRACK, it uses the Melbourne-Wubbena Wide Lane (MW-WL) as an ambiguity resolution to resolve L1-L2 and then a combination of techniques to determine L1 and L2 cycles separately (Melbourne, 1985; Wubbena, 1985). The difference between L1 and L2 phase which the L2 phase scaled to the L1 wavelength is often called simply the wide lane and used to detect cycle slips. However it is affected by fluctuations in the ionospheric delay which is inversely proportional to frequency. The lower frequency L2 has a larger contribution than the higher frequency L1. The MW-WL removes bothe the effects of the ionospheric delay and measures to estimate the difference in phase between L1 and L2,

$$\Phi_{MW-WL} = \Phi_{L1} - \Phi_{L2} - \frac{f_{L1} - f_{L2}}{f_{L1} + f_{L2}}\left[R_{L1} f_{L1} / c + R_{L2} f_{L2} / c \right] \quad (1)$$

Where Φ is the carrier phase, f is frequency, R is pseudorange, term Rf/c is the range in cycles, the $\Delta f / \Sigma f$ term for GPS is 0.124. Because of phase and range biases, the MW-WL should be integer (within noise) when data from different sites and satellites (double differences) are used.

When a baseline is especially long, GAMIT uses floating point estimate with LC combination, L1-L2, and ionospheric delay constant (Hoffmann-Wellenhof et al., 1993),

$$\Phi_{LC} = \frac{f_{L1}^2}{f_{L1}^2 - f_{L2}^2}\Phi_{L1} - \frac{f_{L2}^2}{f_{L1}^2 - f_{L2}^2}\Phi_{L2} \quad (2)$$

Data sampling rate was set 30-seconds. Positions of reference and rover initialize points were determined by the static positioning in advance, and these positions were treated as the "true" positions. Then, the differences between "true" positions and the positions determined by kinematic positioning were measured.

2.2 Results

First, the correlation between the satellite information (number of tracked satellites, satellite alignment) and the kinematic solution is examined (Fig. 3a). Significant differences are not seen among the solutions using different reference points. A phenomenon like a cycle slip is seen, which suggests that receivers at observation points can't track common satellites with low elevation

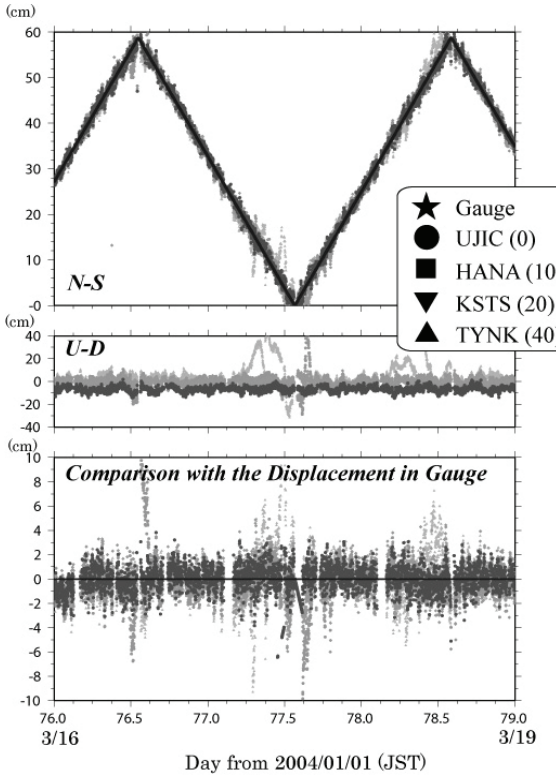

Fig. 4. Comparison of kinematic solutions with the displacements obtained by the gauge. Two upper graphs are the same as those in Fig. 3. The lower graph shows the differences between positions for kinematic GPS and gauge after introducing the zenith tropospheric delay.

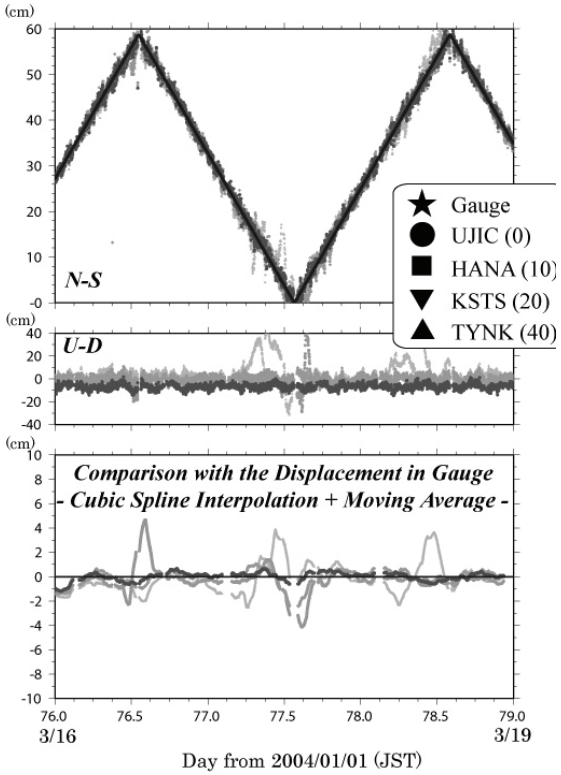

Fig. 5. The graph which shows the time series of position. We removed outliers, and took moving averages with time window of 60 minutes.

angle when baseline length becomes long.

Fig. 3b shows the correlation between the results of kinematic GPS positioning and the ground weather components (atmospheric pressure, temperature, precipitation, humidity, and zenith tropospheric delay).

It isn't seen the correlation between the ground weather components and the positioning accuracy.

Fig. 4 shows comparison with the position analyzed with GAMIT, and the obtained by the displacement gauge. The ionosphere compensation by LC combination and the troposphеic delay obtained at the zero baselines, UJIC, are included in the kinematic analysis, and solution is slightly improved.

Since the GPS observation point moves very slowly, the solution changes smoothly due to the interpolation with a cubic spline functions and moving averages. But, a prediction becomes difficult at the turn of sliding table when we use Kalman filter in the analysis, and solution sometimes becomes irregular. Therefore, solution s are eliminated for thirty minutes before and after the turn, and analyses were done for the time periods between consecutive turns.

We mention the filtering technique of the kinematic analysis result here. First, outlying solutions were removed and interpolated by using cubic spline functions. The threshold to discriminate outliers is described by the model in consideration of the ideal ionospheric delay, ideal tropospheric delay as follows:

$$RESID_{threshold} = (SMBL \times BLL) + MAAPR\_ \quad (3)$$

where *SMBL* is the rough estimate of the measurement value by baseline length, *BLL* is baseline length (km), and *MAAPR* is the average error of the carrier phase to permit it. The parameter that *SMBL* is 1.50 ppm and *MAAPR* is 0.025m used for this kinematic analysis was

Table 3 Maximum, minimum, average, and standard deviation before and after applying cubic spline interpolation and moving averages.

Code	Filtering	Max (cm)	Min (cm)	Average (cm)	STDEV (cm)
UJIC	None	3.815	-6.435	-0.018	1.016
	Only CSI	3.084	-5.440	-0.029	0.914
	Only MA(120)	0.664	-1.215	-0.007	0.384
	CSI + MA (240)	0.474	-1.098	-0.001	0.320
	CSI + MA (60)	0.870	-1.450	-0.026	0.455
	CSI + MA (120)	0.663	-1.211	-0.017	0.386
HANA	None	4.869	-7.162	-0.048	1.305
	Only CSI	4.091	-5.852	-0.068	1.201
	Only MA(120)	1.048	-1.920	-0.034	0.549
	CSI + MA (240)	0.839	-1.428	-0.043	0.494
	CSI + MA (60)	1.416	-2.789	-0.063	0.703
	CSI + MA (120)	1.064	-2.434	-0.054	0.602
KSTS	None	11.137	-12.611	-0.327	1.795
	Only CSI	11.030	-11.321	-0.343	1.728
	Only MA(120)	4.684	-3.707	-0.307	1.021
	CSI + MA (240)	2.460	-2.561	-0.302	0.782
	CSI + MA (60)	7.471	-6.121	-0.330	1.326
	CSI + MA (120)	4.672	-4.138	-0.323	1.055
TYNK	None	12.249	-9.300	-0.183	1.915
	Only CSI	11.846	-8.920	-0.181	1.919
	Only MA(120)	3.651	-2.551	-0.168	1.224
	CSI + MA (240)	2.673	-2.147	-0.143	1.059
	CSI + MA (60)	5.854	-4.199	-0.175	1.462
	CSI + MA (120)	3.891	-2.557	-0.166	1.254

applied here. The time series without outlying solutions is interpolated by cubic spline functions. The coefficients of interpolation were determined by minimizing AIC (Akaike's Information Criterion). Time window for moving average is 60-minute (120 sampling). The result with the moving average with time window for 60-minute and no interpolation with cubic spline functions is shown in Fig. 5. When time window was taken longer than 60-minute, the filtering results became smaller than the actual displacement due to oversmoothing. On the other hand, when time window was taken shorter than 60-minute, we couldn't remove the random error of high frequencies. The statistics for each baseline are shown in the Table 3. In this case, we pay attention to the amount of displacement from the start time of the change. Applying this scheme, the GPS antenna on the sliding table could be tracked with deviation of about +/- 1 cm from the "true position" obtained by the gauge. However, when a warm/cold front passed right above the observation points, positioning accuracy gets worse remarkably (Fig. 6).

2.3 Discussion

We found that a virtual slow event can be observed with an accuracy of +/- 1 cm in this experiment. It is easier to catch anomalous crustal deformations with long baselines, because the amount of relative displacements may be larger as baseline becomes longer. However, since the amount of delay caused in ionosphere and

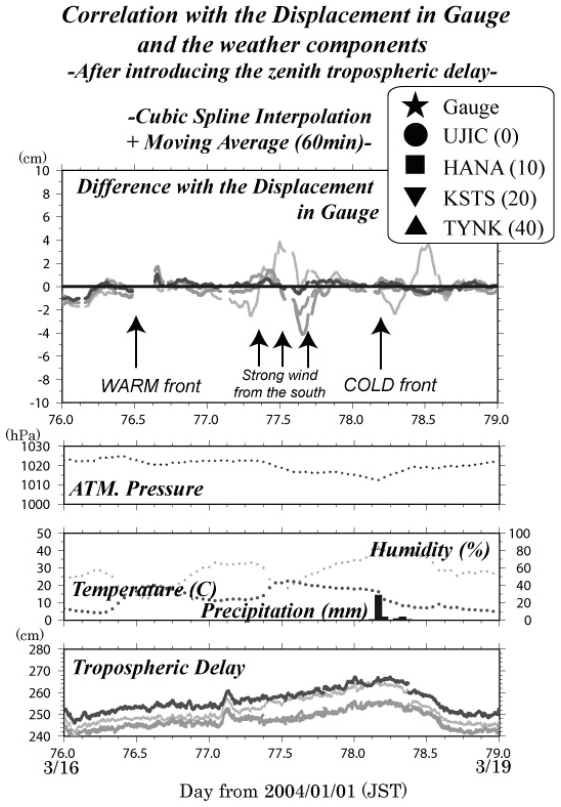

Fig. 6. Correlation between kinematic solutions after moving averages with time window of 60 minutes and the ground weather components. Arrows show the time when the warm/cold frontline passed away above the observation points and strong winds blew from the south.

troposphere grows larger, they bring about large observation errors. Then, we adopted the moving average as a noise reduction. We tried to use Monte Carlo filter (Higuchi, 1997; Fukuda et al., 2004) first. But, an analysis is done by using the Kalman filter which is introduced in GPS analysis software such as GIPSY and GAMIT. We are afraid that the estimated position is far from the true position by passing a filter twice. So we reduced the noise by using the moving average. The maximum, minimum, average, and standard deviation before and after passing through the filter are shown in Table 3. Maximum, minimum approaches the true position drastically in every baseline. Though there was no change in the average, the standard deviation is smaller than before applying the moving average. Though a reduction rate varies in the baseline length, it is greatly reflected as baseline length is short. The systematic error wasn't improved with this technique. Therefore, as for this analysis, we suggest that this technique was suitable.

The tropospheric delay was estimated on the zero baselines at the same time, and an error due to the observation weather elements was reduced by introducing it. It is found that the ground weather was sufficiently reflected in Fig. 6. A decline in the positioning accuracy seen at the time of the warm/cold front suggests that the local weather influences can't be removed when a distance becomes long. In that case, after the tropospheric delay is estimated in advance by the static analysis, random noise can be reduced by applying that value to the kinematic analysis. An anomalous deformation alarm is likely to be raised if we can remove such a disturbance as seen at afternoon on March 17, 2004. Severe wind blew toward a front line from the south side in this time zone. This phenomenon appeared at this time when two points, KSTS and TYNK, vibrated shock because establishment conditions were unstable in these observation points. At the reference point where the antenna is fixed to the pole of 1.5 m with 1 bolt on the roof, it may have kept shaking by the intensive wind. A rover site showed an irregular movement because it is only fixed three points on the side guide-rail of the screw. We think that the dispersion is caused by these two factors. However, this influence will not appear in case of a fixed point like GEONET. Therefore, we don't need to think about such a phenomenon. We pay attention to the change in the local weather, and think that we can get highly accurate position by using this technique. We must develop a local tropospheric model and a filtering technique to remove these phenomena in the future.

3. The experiment of Kinematic GPS positioning with Fixed Stations with long baselines

3.1 Outline of Experiment and Data Analysis

We conducted an experiment with fixed stations to measure the systematic error between static and kinematic positioning using the external frequency standard in Kinki area, Japan, in 2005. The stations and the baselines are shown in Fig.7. We newly established a continuous observation point, Shirahama. These baselines are about 24 km and 141 km, respectively. The receivers are Javad Legacy-E+ external frequency standard and the antennas are Ashtech Dorne-Margolin

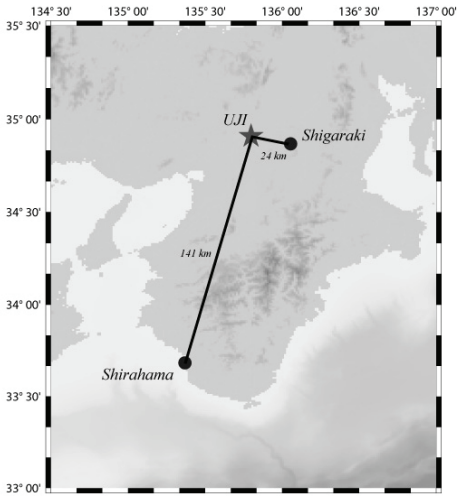

Fig. 7. Baseline map of this experiment. Solid star is a reference point, UJI, and solid circles are observation points, Shigaraki and Shirahama. Baseline lengths are 24, 141 km, respectively.

Choke-ring antenna with SCIGN radome. Data sampling rate was set 30-second. Both reference and rover points were fixed in this experiment. Positions of these points were determined by the static positioning in advance, and these positions were treated as the "true" positions. Then, the differences between these "true" positions and the positions determined by kinematic positioning were measured.

3.2 Spatial Filtering Method

The filtering technique is necessary because baseline length is longer than the previous experiment. As for the analysis, spatial filtering method as the way of detrending, stacking, and filtering was applied. We will describe the method in this section. Spatial filtering method proposed by Wdowinski et al. (1997) consists of three main parts:

Detrending: By a linear regression, determine the best-fit linear trend for each component of coordinate's time series. Tectonic signal is separated from the raw time series as the trend, since it is considered to be long-term continuous change with a spatial gradient. If abrupt change such as coseismic displacement is involved in the time series, the algorithm is applied separately to the data segments before and after the day of change, though this procedure is not necessary in this study. For each day *d* and each site *s*, calculate a residual $\varepsilon^s(d)$ that is a deviation of observed data $O^s(d)$ from the predicted value $C^s(d)$,

$$\varepsilon^s(d) = O^s(d) - C^s(d) \tag{4}$$

We define a data point $O^s(d)$ as the outlier and eliminate it from the time series when $\varepsilon^s(d)$ is larger than three times the root-mean-square of all residuals in the corresponding time series.

Stacking: Calculate a daily common-mode bias $\hat{\varepsilon}(d)$ by averaging residuals from all *N* sites,

$$\varepsilon(d) = \sum_{s=1}^{N} \varepsilon^s(d) / N \tag{5}$$

The minimum criterion of station number used for the stacking is two, that is, when data at all stations but one has been already delected in the step (I) because of large residuals, no error output is obtained on that day. The result may be dependent on the selection of stations, which we will check in the next station.

Filtering: For each day d and each site s, subtract the common-mode bias from the observed position.

$$O^s(d) = O^s(d) - \hat{\varepsilon}(d) \tag{6}$$

Finally determine the best-fit linear trend again for the filtered time series.

3.3 Results

First, Fig.8 shows the correlation between the results of kinematic GPS positioning and the ground weather components (precipitation, humidity, temperature, and zenith tropospheric delay).

It can't be compared with the ground weather components, because the noise of both the horizontal and vertical components is too large. So, we remove the common mode bias using the spatial filter introduced with a previous paragraph. Many error factors are contained in this common mode bias in such cases as the ionosphere and troposphere delay and satellite orbit. Fig. 9 shows the common mode bias in this experiment. When we see Fig. 8 and Fig. 9, it is understood the most of the error factors are common mode bias.

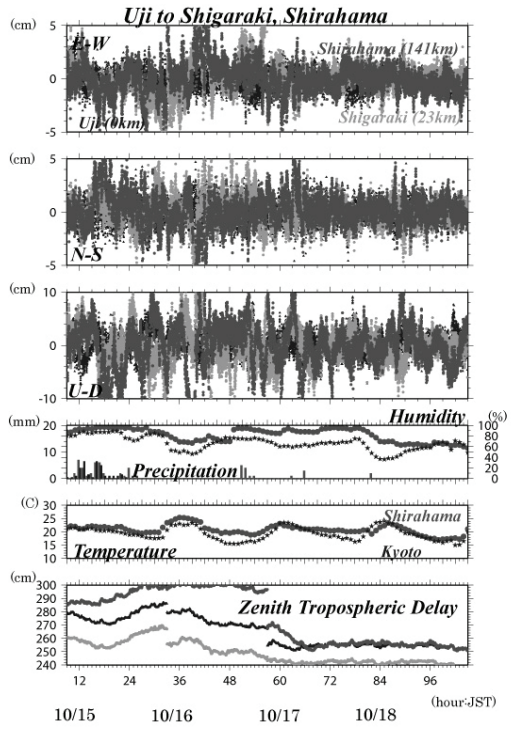

Fig. 8. Correlation between kinematic solutions and the ground weather components.

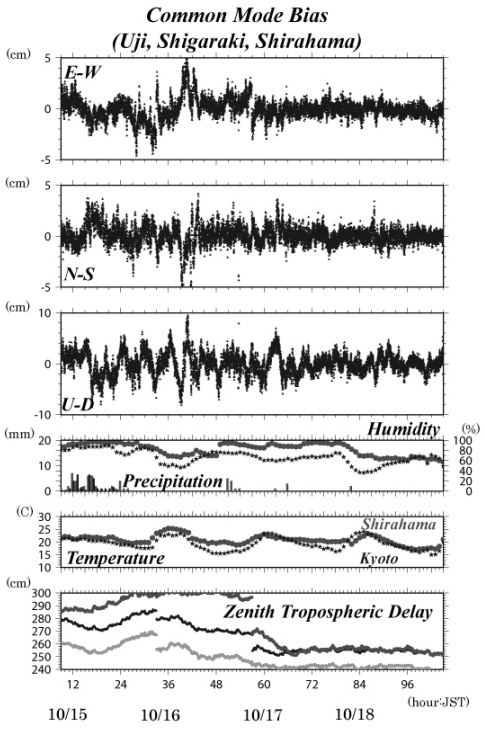

Fig. 9. Correlation between kinematic solutions and the ground weather components.

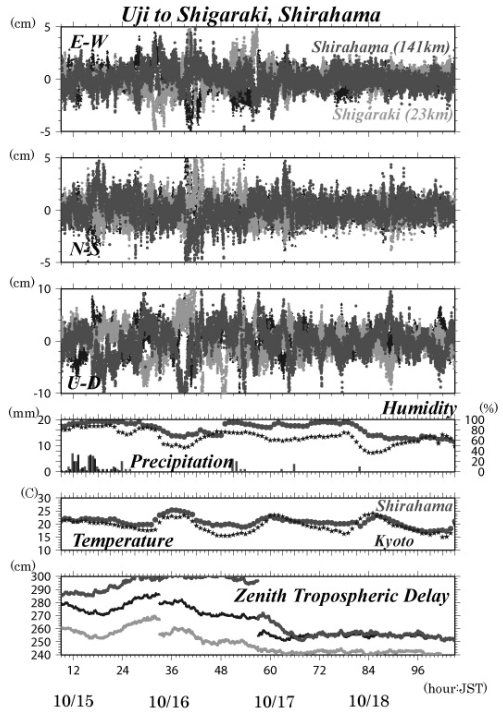

Fig. 10. Comparison of kinematic solutions with the displacement after introducing the spatial filter.

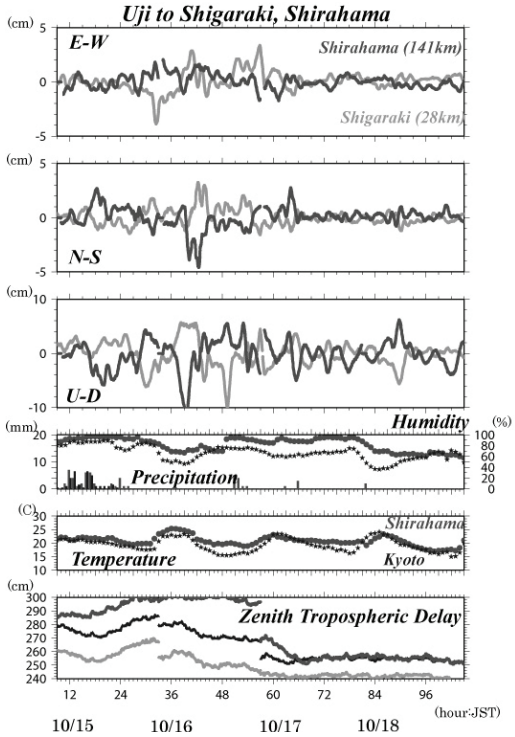

Fig. 11. The graph which shows the time series of position. We took moving averages with time window of 60 minutes.

Table 4 Maximum, minimum, average, and standard deviation before and after applying spatial filter and moving average.

Observation		Filtering	Max (cm)	Min (cm)	Average (cm)	STDEV (cm)
Shigaraki	North	None	10.030	-9.310	0.000	1.466
		Only SF	11.620	-4.630	0.004	1.056
		SF + MA (120)	3.260	-2.160	0.000	0.698
	East	None	9.610	-10.980	0.001	1.692
		Only SF	5.640	-6.770	0.015	1.077
		SF + MA (120)	3.380	-3.890	0.013	0.857
	Up	None	17.960	-20.570	0.001	3.628
		Only SF	13.210	-17.080	-0.019	2.808
		SF + MA (120)	5.740	-9.980	-0.020	2.354
Shirahama	North	None	7.760	-22.520	-0.003	1.768
		Only SF	6.800	-17.280	0.000	1.253
		SF + MA (120)	2.770	-4.590	-0.001	0.854
	East	None	10.020	-7.390	0.004	1.411
		Only SF	5.180	-4.830	0.017	0.951
		SF + MA (120)	2.060	-1.730	0.016	0.593
	Up	None	54.920	-23.000	0.006	4.253
		Only SF	34.050	-16.570	-0.014	3.084
		SF + MA (120)	6.220	-11.150	-0.008	2.480

We show the time series that a common mode biases were removed in Fig. 10. As for the horizontal component, we evaluate positioning accuracy within the range of +/- 2cm that there were no relations with the length of baselines. The result with the moving average with time window for 60-minute is shown in Fig. 11. The statistics for each baseline are shown in the Table 4. It found that standard deviation was restrained small by the adequate filter which we used in every component of every baseline.

3.4 Discussion

We erased an error factor by using the cubic spline function and moving average in the previous chapter. However, the error factor by the ionosphere and the troposphere couldn't be erased completely. If a baseline was extended, it had the possibility that a small anomalous deformation was buried in the noise. We thought about the technique of the more adequate filter before extending a baseline. A spatial filter has already been used in the static analysis technique. Wdowinski et al. (1997) applied it to the result of the Southern California permanent GPS geodetic array in the 1992 Landers earthquake. Tabei and Amin (2002) applied this filter to the daily solution for two years of GEONET. Time-series data was improved drastically, and it extracted a trend and a change easily as well. Hashimoto et al. (2006) applied this method to the Sumatra-Andaman earthquake in 2004 and 2005. The utility of this method was confirmed though a range became wide and observation points were few. The common mode error factor by this technique can't be specified. However, most error factor originates in the carrier phase passes to the observation point from the satellite. Even if it is long, a baseline in the kinematic

positioning is probably about 300km. If it thinks so, a pass from the satellite to the observation point is almost the same to the ground 10-100 km. Therefore, we think that it becomes possible that an error factor is excluded by using this technique only with the ground weather element. Because it doesn't depend on a reference point more till now, it becomes possible that the error factor to originate in the reference point is excluded, too. We will have to evaluate positioning accuracy in the various weather components. So we think that it becomes possible that information will be provided by accumulating the information which is characteristic of the observation point in the future.

4. Satellite Orbit

There are four kinds of satellite orbit. First, a broadcasting ephemeris is put directly in the carrier phase from GPS satellite. It never almost uses in the geodesy because the precision of satellite orbit is bad. Other satellite orbits are published that the International GNSS Service (IGS) calculates every satellite orbit. Announcement times of these satellite orbits are different. An ultra rapid orbit is published in the previous day or the day, the rapid orbit is published after one day, and a precise ephemeris is finally published after two weeks. It thought that positioning accuracy by the precise ephemeris was high now. However, we need to evaluate positioning accuracy by the satellite orbit published fast to monitor crustal deformation in semi-real time. So, we evaluate positioning accuracy by each satellite orbit in the previous experiment. As a example, that result of Uji-Shirahama baseline is shown in Fig. 12. Though a positioning solution by three satellite orbits was shown, as for the horizontal component, positioning solutions almost overlapped, and we ascertained that there were not few differences in the positioning solution by the difference in the satellite orbit.

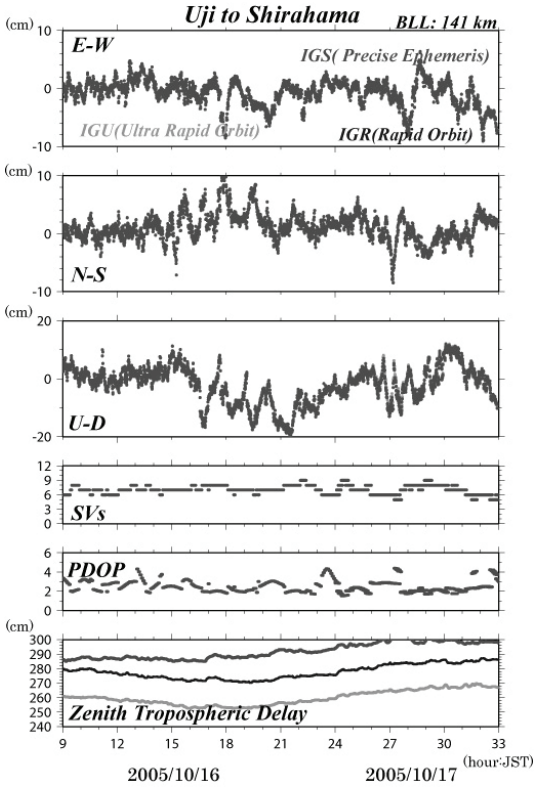

Fig. 12. The influence of the positioning accuracy by the difference in the satellite orbit. Most times overlapped, and A difference in the positioning accuracy is hardly seen.

5. Conclusions

We discussed the error factors to detect an anomalous crustal deformation. Two accuracy verification experiments were done, and we successfully detected the error factors and developed a suitable noise reduction method.

First, we took an influence on the positioning accuracy of the ionospheric and tropospheric delay into consideration. These error factors were reduced by introducing the next two methods: (1) using the LC band which an linear combination of dual-frequency, and (2) estimating the amount of the tropospheric delay by using the static analysis in advance, and introduce that solution in the kinematic analysis. Furthermore, we succeeded in making the solution within +/- 1 cm by applying the cubic spline interpolations and moving averages.

Next, we examined the accuracy with the long baseline consisting of fixed points. As a result, we found that an observation point can be measured the solution within +/- 1 cm by combining the spatial filter and moving averages even if a baseline becomes long.

Finally, we evaluated a difference in the positioning accuracy by the difference in the satellite orbit. A large difference wasn't seen in the positioning accuracy in every satellite orbit published from IGS.

From the above, if data were accumulated by using a suitable filter and IGS rapid orbit, we found that it was possible that an anomalous crustal deformation was detected in the future.

Acknowledgements

We obtained GPS RINEX data from Ocean Bottom Crustal Deformation Observation Group of Nagoya University and Geographical Survey Institute of Japan, which is appreciated.

References

Bock, Y., L. Prawirodirdjo, and T. I. Melbourne (2004): Detection of arbitrarily large dynamic ground motions with a dense high-rate GPS network, Geophys. Res. Lett., Vol. 31, L06604, doi:10.1029/2003GL019150.

Fukuda, J., T. Higuchi, S. Miyazaki, and T. Kato (2004): A new approach to time-dependent inversion of geodetic data using Monte Carlo mixture Kalman filter, Geophys. J. Int., Vol. 159, pp. 17-39.

Hashimoto, M., N. Chhoosakul, M. Hashizume, S. Takemoto, H. Takiguchi, Y. Fukuda, and K. Fujimori (2006): Crustal deformations associated with the great Sumatra-Andaman earthquake deduced from continuous GPS observation, submitted by Earth Planets. Space.

Higuchi, T. (1997): Monte Carlo filter using the Genetic algorithm operators, J. Statistical Computation and Simulation, Vol. 59, No. 1, pp. 1-23.

Hoffmann-Wellenhof, B., H. Lichtenegger, J. Collins, GPS Theory and Practice, 4th edition, Springer, Wien-New York, 382.pp.

Irwan, M., F. Kimata, N. Fujii, S. Nakao, H. Watanabe, S. Sakai, M. Ukawa, W. Fujita, and K. Kawai (2003): Rapid ground deformation of the Miyakejima volcano on 26-27 June 2000 Detected by Kinematic GPS analysis, Earth Planets Space, Vol. 55, pp. e13-e16.

King, R. W. et al. (2002): Documentation for the GAMIT GPS Analysis Software: Release 10.0, Masachusetts Institute of Technology and University of California at San Diego.

Lachapelle, G., M.E. cannon, and G. Lu (1992): High-Precision GPS Navigation with Emphasis on Carrier-Phase Ambiguity Resolution, Marine Geodesy, Vol. 15, pp. 253-269

Larson, K. M., P. Cervelli, M. Lisowski, A. Miklius, P. Segall and S. Owen (2001): Volcano monitoring using the Global Positioning System: strategies, J. Geophys. Res., Vol. 106, pp. 19453-19464.

Larson, K. M., P. Bodin and J. Gomberg (2003): Using 1-Hz GPS Data to Measure Deformations Caused by the Denali Fault Earthquake, Science, Vol. 300, pp. 1421-1424.

Lichten, S. M., and J.S. Border (1987): Strategies for High-Precision Global Positioning System, J. Geophys. Res., Vol. 92, pp. 12751-12762.

Melbourne, W.G. (1985): The Case for Ranging in GPS Based Geodetic Systems, Proceedings 1st International Symposium on Precise Positioning with the Global Positioning System, edited by Clyde Goad, Earth. Planet. Sci. Lett., pp. 403-412, U.S. Department fo Commerce, Rockville, Maryland.

Mogi, K. (1982): Temporal variation of the precursory crustal deformation just prior to the 1944 Tonankai earthquake, J. Seismol. Soc. Japan, Vol. 35, pp. 145-148.

Mogi, K. (1985): Temporal variation of crustal deformation during the days preceding a thrust-type great earthquake – the 1944 Tonankai earthquake of magnitude 8 in Japan, Pure Appl. Geophys., Vol. 122, pp. 765-780.

Nikolaidis, R.M., Y. Bock, P.J. Jonge, P. Shearer, D.C. Agnew, and M. Domselaar (2001): Seismic wave observations with the Global Positioning System, J. Geophys. Res., Vol. 106, pp. 21897-21916.

Obana, K., H. Katao, and M. Ando (1999): Sea floor positioning with GPS-acoustic link system, The Islands Arc, Vol. 8, pp. 245-258.

Sato, K. (2002): Improvement of Position Determination Accuracy by Long-Baseline Kinematic GPS Positioning – For the Highly Precise Ocean Bottom Crustal Deformation Monitoring in Subduction Zones, Master Thesis, Department of Geophysics, Graduate School of Science, Kyoto University, 60pp.

Tabei, T., and Amin, W. L. (2002): Common-mode Errors in the GPS Coordinates Time Series –Application of Spatial Filtering Technique-, J. Geod. Soc. Japan, Vol. 48, No. 4, pp. 229-241.

Tsuchiya, J., and H. Tsuji (1995): The Basic of GPS Survey, Japan Association of Surveyors, Tokyo, Japan, 338pp.

Wdowinski, S., Y. Bock, J. Zhang, P. Fang, and J. Genrich (1997): Southern California Permanent GPS Geodetic Array: Spatial filtering of daily positions for

estimating coseismic and postseismic displacements induced by the 1992 Landers earthquake, J. Geophys. Res., Vol. 102, pp. 18057-18070.

Wubbena, G. (1985): Software Developments for Geodetic Positioning with GPS Using TI 4000 Code and Carrier Measurements, Proceedings 1st International Symposium on Precise Positioning with the Global Positioning System, edited by Clyde Goad, J. Geophys. Res., pp. 403-412, U. S. Department of Commerce, Rockville, Maryland.

Zumberge, J.F., M.B. Heflin, D.C. Jefferson, M.M. Watkins, and F.H. Webb (1997): Precise point positioning for the efficient and robust analysis of GPS data from large networks, J. Geophys. Res. Vol. 102, pp. 5005-5017.

異常地殻変動検出手法の開発

佐藤一敏・橋本　学・細　善信

要旨

我々は異常地殻変動検出手法の開発に取り組んでいる。時定数の短い変動を捉えるためには，キネマティック測位を応用した手法を用いて，電離層や対流圏遅延などの誤差要因を除去しなければならない。これらを移動平均によって±1㎝の精度まで取り除くことができた。さらに長基線に展開するため，新たに空間フィルター法を適用し共通誤差成分を取り除くことによって，基線の長さに関係なく±1㎝の精度で議論できるようになった。また衛星軌道暦の違いによる測位精度への影響はほとんどないので，準リアルタイムモニタリングシステムの構築が可能になった。

キーワード:電離層遅延，対流圏遅延，移動平均，空間フィルター，衛星軌道暦